Unveiling the underlying interactions in Ta$_2$NiSe$_5$ from photoinduced lifetime change

Denis Golež [1,2,3,*] Sydney K. Y. Dufresne [4,5,*] Min-Jae Kim,[6,7,8] Fabio Boschini,[4,5,9] Hao Chu,[4,5,6] Yuta Murakami [10]
Giorgio Levy,[4,5] Arthur K. Mills [4,5] Sergey Zhdanovich [4,5] Masahiko Isobe [6] Hidenori Takagi,[6,10] Stefan Kaiser [6,7,8]
Philipp Werner,[11] David J. Jones,[4,5] Antoine Georges [3,12,13,14] Andrea Damascelli,[4,5] and Andrew J. Millis[3,15]

[1]*Jozef Stefan Institute, Jamova 39, SI-1000 Ljubljana, Slovenia*
[2]*Faculty of Mathematics and Physics, University of Ljubljana, Jadranska 19, SI-1000 Ljubljana, Slovenia*
[3]*Center for Computational Quantum Physics, Flatiron Institute, 162 Fifth Avenue, New York, New York 10010, USA*
[4]*Quantum Matter Institute, University of British Columbia, Vancouver, British Columbia, Canada V6T 1Z4*
[5]*Department of Physics & Astronomy, University of British Columbia, Vancouver, British Columbia, Canada V6T 1Z1*
[6]*Max Planck Institute for Solid State Research, Heisenbergstrasse 1, D-70569 Stuttgart, Germany*
[7]*4th Physics Institute, University of Stuttgart, D-70569 Stuttgart, Germany*
[8]*Institut für Festkörper- und Materialphysik, Technische Universität Dresden, D-01069 Dresden, Germany*
[9]*Centre Énergie Matériaux Télécommunications, Institut National de la Recherche Scientifique, Varennes, Québec, Canada J3X 1S2*
[10]*Department of Physics, Tokyo Institute of Technology, Meguro, Tokyo 152-8551, Japan*
[11]*Department of Physics, University of Fribourg, CH-1700 Fribourg, Switzerland*
[12]*Collège de France, 11 place Marcelin Berthelot, F-75005 Paris, France*
[13]*CPHT, CNRS, Ecole Polytechnique, IP Paris, F-91128 Palaiseau, France*
[14]*Department of Quantum Matter Physics, University of Geneva, CH-1211 Geneva 4, Switzerland*
[15]*Department of Physics, Columbia University, 538 West 120th Street, New York, New York 10027, USA*

We present a generic procedure for quantifying the interplay of electronic and lattice degrees of freedom in photodoped insulators through a comparative analysis of theoretical many-body simulations and time- and angle-resolved photoemission spectroscopy (TR-ARPES) of the transient response of the candidate excitonic insulator Ta$_2$NiSe$_5$. Our analysis demonstrates that the electron-electron interactions dominate the electron-phonon ones. In particular, a detailed analysis of the TR-ARPES spectrum enables a clear separation of the dominant broadening (electronic lifetime) effects from the much smaller band-gap renormalization. Theoretical calculations show that the observed strong spectral broadening arises from the electronic scattering of the photoexcited particle-hole pairs and cannot be accounted for in a model in which electron-phonon interactions are dominant. The competing interactions were quantified using the scaling analysis in the weak fluence regime. We demonstrate that the magnitude of the weaker subdominant band-gap renormalization sensitively depends on the distance from the semiconductor/semimetal transition in the high-temperature state, which could explain the apparent contradictions between various TR-ARPES experiments. The analysis presented here indicates that electron-electron interactions play a vital role (albeit not the sole one) in stabilizing the insulating state, and establishes the comparison between lifetime and gap evolution as an important probe of correlated insulators.

The essence of strongly correlated electron physics is understanding how novel ground states, such as high-temperature superconductivity, charge orders, and excitonic insulator (EI) behavior as paradigmatic examples, emerge from competing degrees of freedom [1]. The excitonic insulator is a quantum many-body state involving electron-hole pairing which can appear in semimetals or narrow gap semiconductors [2–6]. In the semiconducting case, the excitonic binding energy exceeds the single particle gap leading to the Bose-Einstein condensation (BEC) of excitons. In the semimetallic case, the phase transition is described as a binding of weakly interacting electron-hole pairs [5,7] in analogy to the binding of electron-electron pairs described

in the Bardeen-Cooper-Schrieffer (BCS) theory of superconductivity. However, in solid state systems, an EI is typically strongly coupled to lattice degrees of freedom and the interplay between electronic and electron-phonon interactions is a recurrent question in the field [8–14].

Recently, several systems have been proposed as excitonic insulator candidates, including 1T-TiSe$_2$ [15,16], Ta$_2$NiSe$_5$ (TNS) [17–20], WTe$_2$ [21], and Sb nanoflakes [22]. These materials have been the subject of extensive experimental exploration [8,10,11,15,23–25] and theoretical modeling [26–28], in an effort to provide definitive confirmation on the existence of the excitonic ground state and to elucidate the plethora of unique electronic and optical properties [29–32]. TNS has been of particular interest in this context. The characteristic flattening of the valence band observed by angle-resolved photoemission spectroscopy (ARPES) [19,33]

---

suggests a BCS pairing interpretation of the insulating state, while the possibility of tuning the BCS-BEC transition via chemical or physical pressure [17] opens new avenues for experimental investigation.

Early equilibrium ARPES results on TNS were interpreted within a purely electronic picture [24,28,34], but subsequent additional experimental probes, including Raman [8–11] and optical spectroscopy [25,35–37], have suggested a strong coupling between the EI and lattice distortions, raising the question of the quantitative contribution of the electronic and lattice instabilities to the opening of the gap in TNS. To resolve this question, time-resolved ARPES (TR-ARPES) experiments have focused on the ultrafast response of the electronic gap, reporting either a transient modulation of the gap amplitude (interpreted within an electronic picture [13,38,39]) or a rigid gap response (interpreted within a largely lattice-driven scenario [12]).

Theoretical developments have followed a similar trajectory, where initial studies have focused on a purely excitonic description that successfully reproduced the equilibrium ARPES spectrum of TNS [28,33] and optical absorption spectra [40]. However, subsequent studies have revealed the importance of the electron-lattice coupling [12,41,42], and the interplay between electron-electron and electron-phonon contributions is currently debated with nonlinear optical responses [25,37,43], collective dynamics [26,44], and transient protocols for the order enhancement [45–48], all discussed as highlighting either the electron-electron or electron-lattice contributions to the excitonic insulator state.

Motivated by these challenges, we performed a comparative analysis of photodoped TNS using TR-ARPES and realistic model-system nonequilibrium many-body calculations that treat electronic and lattice degrees of freedom on equal footing. We focus on the weak-to-intermediate photoexcitation regime and show that the experimental response after photoexcitation is dominated by strong spectral broadening within the excitonic gap, which is well captured by microscopic simulations in the scenario of dominant electron-electron interactions.

TR-ARPES measurements were performed at the UBC-Moore Center for Ultrafast Quantum Matter by pumping with 1.55 eV photons (with incident fluence ranging from 26 to 160 μJ/cm^2), and probing with 6.2 eV photons at a repetition rate of 250 kHz. The samples were aligned by Laue diffraction prior to the TR-ARPES measurements, and cleaved at 95 K in UHV at a base pressure better than 5×10^{-11} Torr. All TR-ARPES experiments were performed at a base cryostat temperature of 95 K; however, pump-induced thermal effects raising the sample's effective base temperature have to be taken into account independently for each experiment. Both pump and probe beams were polarized parallel to the Ta-Ni chain direction, and the overall time and energy resolution of the system were 250 fs and 11 meV, respectively [49].

The equilibrium spectra [Fig. 1(a)] show a characteristic "M"-like flat upper valence band (UVB) centered at Γ, a dispersion that is characteristic of the EI ground state in the BCS regime [50,51]. Upon photoexcitation, we observe a significant decrease of the spectral weight. The response is clearly dominated by the UVB's broadening and to a lesser extent by a change in the peak position, as shown by com-
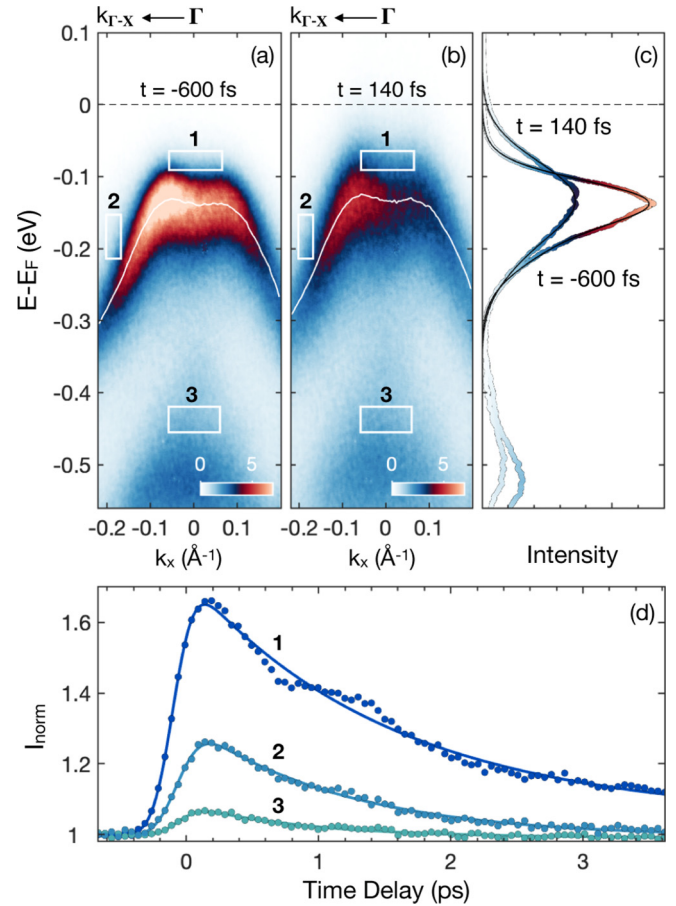
FIG. 1. TR-ARPES data acquired along the Γ-*X* direction (a) before ($t = -600$ fs) (b) and after ($t = 140$ fs) photoexcitation with a 50 μJ/cm^2 incident pump fluence. (c) EDCs centered at Γ before and after photoexcitation. (d) Time dependence of the integrated photoemission intensity over the three energy momentum regions outlined in white in (b) normalized to the equilibrium photoemission intensity in the corresponding regions in (a).

parison of the photoemission spectra in Figs. 1(a) and 1(b) (regions 1 and 2), and in the energy distribution curves (EDCs) presented in Fig. 1(c). We quantify the two contributions by extracting the full width at half maximum (FWHM) and the peak position E_0 from a fit to the UVB EDC spectral line shape [the solid black line in Fig. 1(c) is the fit curve—see details in the Supplemental Material [52]].

We analyze characteristic timescales of photoinduced effects by simple visualization of the energy- and momentum-integrated spectral intensity in selected areas as a function of pump-probe delay [see Fig. 1(d)]. Each area is outside of the main band region, and all show a clear pump-induced increase in spectral intensity shortly after photoexcitation, followed by an exponential decay with a superimposed ∼1 THz oscillation observed in all areas. The latter is most apparent in region 1, approximately 1 ps after photoexcitation. Note that additional higher-frequency phonons were observed in previous studies [12,39,53], but are not seen here due to the pulse duration in our experiments being too long to effectively excite those modes [54].
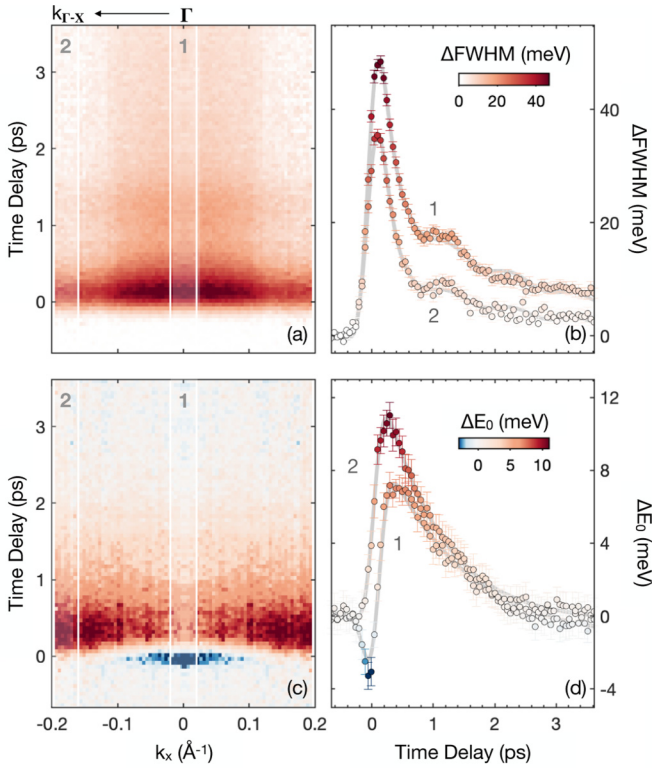
FIG. 2. (a) Momentum- and time-dependent change of the UVB width ΔFWHM(k_x, t) for a 50 μJ/cm^2 incident fluence. (b) One-dimensional traces of the UVB width as a function of pump-probe delay taken from momentum integrated regions at Γ (region 1), and at higher momenta (region 2), outlined by the white shaded areas in (a). (c), (d) Analog plots for the momentum- and time-dependent change in the UVB position $\Delta E_0(k_x, t)$ with positive (negative) values corresponding to the gap decrease (increase).

The time- and momentum-dependent ΔFWHM of the UVB is displayed in Fig. 2(a), with selected traces around the Γ point (region 1), and at the highest momenta measured (region 2) in Fig. 2(b). From Figs. 2(a) and 2(b), one can observe a significant change in the broadening and relatively uniform rise time across the entire k_x region acquired, and subsequent relaxation with a superimposed $\sim$1 THz oscillation. The change in the gap amplitude [Figs. 2(c) and 2(d)], in terms of a relative shift in the UVB position, shows a significantly different time dependence than the linewidth. Unlike the width, the peak position shows no evidence of the $\sim$1 THz oscillation. This indicates that the oscillation observed in the normalized transient photoemission intensity [Fig. 1(d), box 1 and 2] is a product of the UVB broadening and not an oscillation in the gap amplitude. Around Γ, the renormalization shows a nonmonotonic response to photoexcitation, with a short-lived ($\sim$200 fs) resolution-limited gap enhancement [downward shift in the UVB position to higher binding energies $\Delta E_0(k_x, t) < 0$], which is qualitatively consistent with Ref. [13]. The enhancement is followed by a partial gap closure [upward relative shift in the UVB position to lower energies, $\Delta E_0(k_x, t) > 0$], ending with an exponential recovery to equilibrium. On the contrary, we do not observe an ultrafast enhancement of the gap at higher mo-

menta. The UVB shifts towards the Fermi level by a maximum of 11 meV (on the order of the energy resolution). In summary, the pump-induced modifications to the photoemission spectrum are dominated by the UVB broadening, which is nearly an order of magnitude larger than the contribution of the band-gap renormalization.

From here, we turn to theoretical modeling to qualitatively understand the microscopic implications of the observation. The model consists of two-band spinless fermions in one dimension coupled to dispersionless phonons:

$$
\begin{aligned}
H = &\sum_{k, \alpha, \alpha' \in \{0,1\}} [\epsilon_{k-A}]^{\alpha\alpha'} c_{k,\alpha}^\dagger c_{k,\alpha'} + V \sum_i n_{i,0} n_{i,1} \\
&+ \sum_i [\sqrt{\lambda} X_i - E(t)] c_{k,0}^\dagger c_{k,1} + \sum_i \frac{1}{2}\left[X_i^2 + \frac{1}{\omega_0^2} \dot{X}_i^2 \right] \\
&+ \text{H.c.},
\end{aligned} \tag{1}
$$

where $c_{k,\alpha}^\dagger$ is the electron creation operator for band α at momentum k, V is the Coulomb interaction strength between the conduction and valence band, λ is the electron-phonon interaction strength corresponding to a displacement of $X = X_i$, and $E(A)$ is the electric field (vector potential) [55–57]. The dispersion relation ϵ_k is obtained from the Wannier-interpolated density functional theory (DFT) band structure in the high-temperature orthorhombic phase [34]. We mapped the Ta-Ni-Ta chain to the two-band problem by neglecting the interchain hopping as the smallest energy scale in the system [52].

Note that for all calculations presented, we include a weakly coupled bosonic bath not explicitly written in Eq. (1), so that the photoinduced electrons (holes) within the maximum propagation time relax to the lower (upper) edge of the conduction (valence) band for all parameters.

The analysis of the photoinduced change in the lifetime calls for the inclusion of excitonic and lattice fluctuations on equal footing. We employ the Keldysh formalism with the second Born (Migdal) approximation for the electron-electron (electron-lattice) scattering directly in the excitonic phase [52]. First of all, we reproduce the experimental gap in equilibrium for various relative strengths of the electronic V and electron-lattice interactions λ at a fixed gap size $2\Delta = 0.25$ eV, and distinguish the electronically dominated ($V \gg \lambda$) and lattice dominated ($V \ll \lambda$) case. Afterwards, we estimate the relative importance of V and λ by analyzing photoinduced changes in the spectrum.

The system is excited by an electric field parametrized as $E(t) = A_0 \sin(\Omega t) e^{-4.2(t-t_0)^2}$, where A_0 is the pump strength, Ω is the 1.5 eV pump energy, and t_0 determines the single-cycle pump pulse. We adjust the pump strength A_0 such that the number of photoexcited electrons is fixed to Δn. The comparison between the theoretical [52] and the experimentally determined photoemission EDCs $I(\omega, k_x)$ for different momenta, before and after ($t_p = 140$ fs) photoexcitation, are presented in Fig. 3. Experimental data have been acquired at a repetition rate of 250 kHz, and steady-state heating of the sample has been observed and quantified for each fluence. The theoretical base temperature for higher fluences is adjusted by fixing the gap size to the experimental value before the pump pulse (see details in Supplemental Material [52]). The
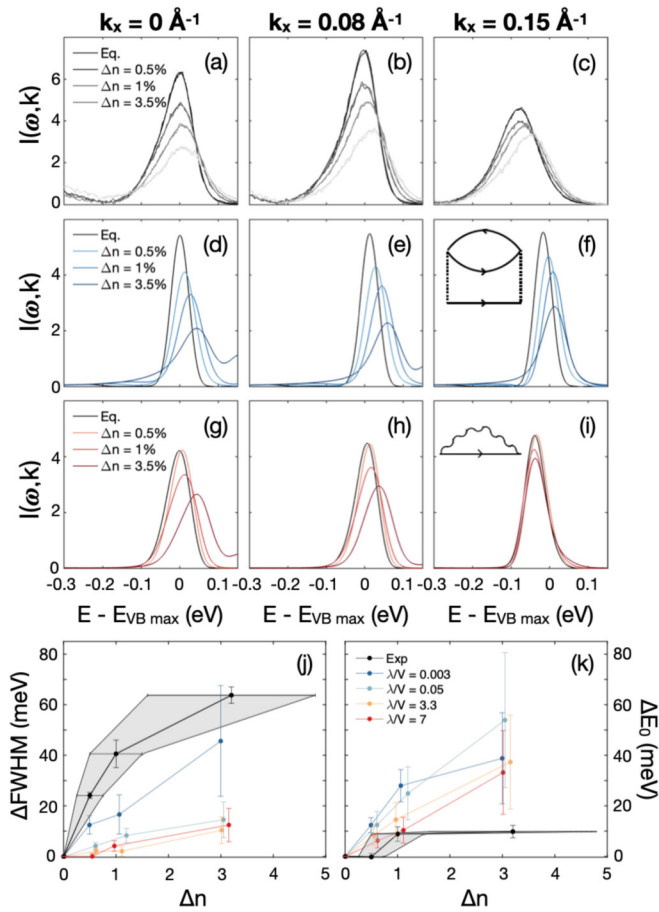
FIG. 3. Comparison of the photoemission spectrum in equilibrium (Eq) and $t_p = 140$ fs after the photoexcitation at three characteristic momenta along the Γ-X direction, namely $k_x = 0$ (first column), $k_x = 0.08$ Å^{-1} (second column), and $k_x = 0.15$ Å^{-1} (third column), and for different excitation strengths [$\Delta n = 0.5\%$ (26 μJ/cm^2), 1% (50 μJ/cm^2), 3.5% (160 μJ/cm^2)]. (a)–(c) Experimental EDCs. (d)–(f) and (g)–(i) Theoretical results in the electron ($V = 0.76$ eV, $\lambda = 0.03$ eV, and $\omega_0 = 0.016$ eV) and the lattice ($V = 0.17$ eV, $\lambda = 0.33$ eV, and $\omega_0 = 0.016$ eV) dominated regime, respectively. The inset presents the lowest-order scattering diagram for the two characteristic regimes. (j), (k) The experimental and the theoretical change in width ΔFWHM (j) and position ΔE_0 (k) of the UVB as a function of photodoping Δn. Experimental error bars represent an uncertainty in the photodoping estimation leading to theoretical uncertainties obtained from simulations at extreme values.

theoretically derived line profiles were determined for two characteristic regimes: (i) the primarily electron-driven case ($V = 0.92$ eV, $\lambda = 0.03$ eV), and (ii) the primarily lattice-driven case ($V = 0.13$ eV, $\lambda = 0.43$ eV).

In equilibrium, the width of the UVB is consistently larger in the experimental data [black curves in Figs. 3(a)–3(c)] than in the theoretical predictions. This is likely to originate from the presence of additional scattering channels (different phonons, impurities, etc.). By a simple visual comparison of the nonequilibrium results in Fig. 3, we note that the significant broadening of the UVB is only captured in the primarily electron-driven case [Figs. 3(d)–3(f)]. In contrast, the transient variation of the width in the lattice-driven case is substantially smaller.

We compare the theoretical and experimental results more quantitatively by extracting the photoinduced change in the width (ΔFWHM), proportional to the quasiparticle lifetime change, and the peak position (ΔE_0) of the UVB EDC centered at Γ as a function of photodoping Δn [52]. We note that, although experimental and theoretical ΔFWHM display different absolute variations, the trend as a function of the photoexcitation density is better captured by the pure electronic-driven case [see Fig. 3(j) (blue curve)]. Note particularly that in the primarily phonon-driven case, the linewidth displays only a weak dependence on the photodoping excitation, in sharp contrast to experiment.

An analogous comparison for the subdominant band-gap renormalization ΔE_0 is presented in Fig. 3(k). The photoinduced modification in the band position is smaller than the lifetime change. There is an apparent saturation at larger photodoping ($\Delta n > 0.01$) in the experimental data [black data, Fig. 3(k)], which notably occurs below our system energy resolution of 11 meV. Although the experimental and theoretical shifts agree for the smallest photodoping considered ($\Delta n \leqslant 1\%$), the theoretically derived results do not saturate and lead to larger band-gap renormalization.

We now discuss the possible microscopic origins of these observations. The photoexcitation introduces mobile charge carriers into the conduction and valence bands, changing effectively the system's scatterings. The change in the electronic scattering is proportional to the number of photodoped charge carriers which modifies the particle-hole bubble in the lowest-order scattering diagram [see the inset of Fig. 3(f)]. On the contrary, the lowest-order electron-phonon scattering [see the inset of Fig. 3(i)] can be estimated from the Fermi golden rule as $\Sigma(\omega) \propto \lambda\rho(\omega - \omega_0)$, where neither the electronic density of states $\rho(\omega)$ nor λ has a direct photodoping dependence, resulting in an electron lattice scattering rate with a weak dependence on the photoexcitation intensity. While the self-consistent Migdal approximation allows for the dressing of the lattice propagator, our numerical results show that the broadening is small and primarily originates from heating effects due to the finite repetition rate. Therefore, the qualitative difference in the lifetime scaling can be ascribed to the distinct scatterings between the electronic and lattice degrees of freedom. The qualitative agreement between the experimental and theoretical photodoping dependence of the lifetime suggests a robust electronic character in TNS.

Finally, the experimental band-gap renormalization close to the Γ point is, surprisingly, small; importantly, we even observed a transient enhancement [see Fig. 2(c)]. We investigated the gap size evolution after a nonlinear excitation, and we show that it is highly susceptible to the position in the BCS-BEC crossover [51], as revealed by the dynamics of the excitonic order parameter $\phi = \sum_k \langle c_{1,k}^\dagger c_{0,k} \rangle$ being a direct measure of the gap size. In the (semimetallic) BCS regime, we report a monotonic reduction of the order parameter upon optical excitation [see Fig. 4(a)]. On the contrary, a transient enhancement of order parameter can be observed in the (semiconducting) BEC regime [Fig. 4(b)], in agreement with the experimental findings [Fig. 2(d)]. The enhancement is only transient due to the inclusion of scatterings, in contrast to previous time-dependent mean-field studies predicting a long-lasting enhancement [45–48]. The implications of these
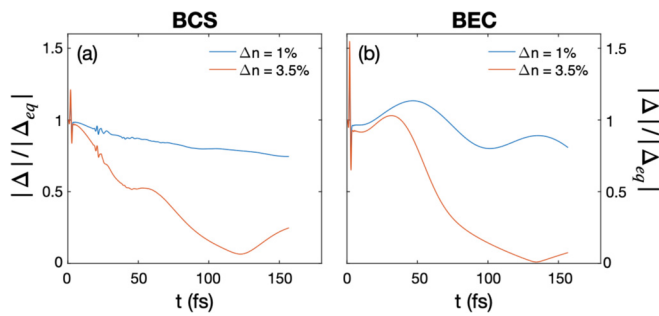
FIG. 4. Time dependence of the order parameter in (a) the BCS and (b) the BEC regime after a photoexcitation for different excitation strengths.

results are twofold. First, the sensitivity of the gap renormalization dynamics to the position in the BEC-BCS crossover may explain the apparent contradiction between theory and experiment in Fig. 3(k), as well as various TR-ARPES experiments which showed a wide range of responses, including gap reductions [38,39,58], gap enhancements [13], and rigid gap shifts [12]. Second, the contradiction between equilibrium ARPES results, suggesting a BCS nature of the ground state, and the transient gap enhancement observed in TR-ARPES, remains an open question.

In conclusion, we have reported a marked photoinduced broadening of the valence band of TNS, while the band-gap renormalization is almost an order of magnitude smaller. A detailed comparison of the TR-ARPES experimental data with nonequilibrium many-body simulations demonstrates the pivotal (but not necessarily sole) contribution of electron-electron interactions to the stabilization of the excitonic gap in TNS.

More broadly, this work demonstrates a generic way to determine the origin of the gap in correlated insulators by analyzing the lifetime effects of photodoped states. Furthermore, the band-gap enhancement after a nonlinear excitation shows a subtle dependence on the position in the BCS-BEC crossover. In this regard, we propose a systematic study of the nonlinear response by applying either chemical or physical pressure, as performed in recent transport [17,59] and Raman measurements [11], to optimize the nonthermal enhancement of the underlying order.

[1] B. Keimer and J. Moore, Nat. Phys. **13**, 1045 (2017).

[2] L. Keldysh and Y. V. Kopaev, Sov. Phys. - Solid State **6**, 2219 (1965).

[3] L. V. Keldysh and A. N. Kozlov, Sov. Phys. - JETP **27**, 521 (1968).

[4] J. D. Cloizeaux, J. Phys. Chem. Solids **26**, 259 (1965).

[5] D. Jérome, T. M. Rice, and W. Kohn, Phys. Rev. **158**, 462 (1967).

[6] W. Kohn, Phys. Rev. Lett. **19**, 439 (1967).

[7] B. Halperin and T. Rice, in *Solid State Physics*, Vol. 21 (Elsevier, Amsterdam, 1968), pp. 115–192.

[8] M.-J. Kim, A. Schulz, T. Takayama, M. Isobe, H. Takagi, and S. Kaiser, Phys. Rev. Research **2**, 042039(R) (2020).

[9] K. Kim, H. Kim, J. Kim, C. Kwon, J. S. Kim, and B. J. Kim, Nat. Commun. **12**, 1969 (2021).

[10] P. A. Volkov, M. Ye, H. Lohani, I. Feldman, A. Kanigel, and G. Blumberg, npj Quantum Mater. **6**, 52 (2021).

[11] M. Ye, P. A. Volkov, H. Lohani, I. Feldman, M. Kim, A. Kanigel, and G. Blumberg, Phys. Rev. B **104**, 045102 (2021).

[12] E. Baldini, A. Zong, D. Choi, C. Lee, M. H. Michael, L. Windgaetter, I. I. Mazin, S. Latini, D. Azoury, B. Lv, A. Kogar, Y. Wang, Y. Lu, T. Takayama, H. Takagi, A. J. Millis, A. Rubio, E. Demler, and N. Gedik, arXiv:2007.02909.

[13] S. Mor, M. Herzog, D. Golež, P. Werner, M. Eckstein, N. Katayama, M. Nohara, H. Takagi, T. Mizokawa, C. Monney, and J. Stähler, Phys. Rev. Lett. **119**, 086401 (2017).

[14] S. Mor, M. Herzog, J. Noack, N. Katayama, M. Nohara, H. Takagi, A. Trunschke, T. Mizokawa, C. Monney, and J. Stähler, Phys. Rev. B **97**, 115154 (2018).

[15] C. Monney, G. Monney, P. Aebi, and H. Beck, New J. Phys. **14**, 075026 (2012).

[16] C. Monney, H. Cercellier, F. Clerc, C. Battaglia, E. F. Schwier, C. Didiot, M. G. Garnier, H. Beck, P. Aebi, H. Berger, L. Forró, and L. Patthey, Phys. Rev. B **79**, 045116 (2009).

[17] Y. Lu, H. Kono, T. Larkin, A. Rost, T. Takayama, A. Boris, B. Keimer, and H. Takagi, Nat. Commun. **8**, 14408 (2017).

[18] S. A. Sunshine and J. A. Ibers, Inorg. Chem. **24**, 3611 (1985).

[19] Y. Wakisaka, T. Sudayama, K. Takubo, T. Mizokawa, M. Arita, H. Namatame, M. Taniguchi, N. Katayama, M. Nohara, and H. Takagi, Phys. Rev. Lett. **103**, 026402 (2009).

[20] Q. He, X. Que, L. Zhou, M. Isobe, D. Huang, and H. Takagi, Phys. Rev. Research **3**, L032074 (2021).

[21] Y. Jia, P. Wang, C.-L. Chiu, Z. Song, G. Yu, B. Jäck, S. Lei, S. Klemenz, F. A. Cevallos, M. Onyszczak *et al.*, Nat. Phys. **18**, 87 (2022).

[22] Z. Li, M. Nadeem, Z. Yue, D. Cortie, M. Fuhrer, and X. Wang, Nano Lett. **19**, 4960 (2019).

[23] Z. Wang, D. A. Rhodes, K. Watanabe, T. Taniguchi, J. C. Hone, J. Shan, and K. F. Mak, Nature (London) **574**, 76 (2019).

[24] M. D. Watson, I. Marković, E. A. Morales, P. Le Fèvre, M. Merz, A. A. Haghighirad, and P. D. C. King, Phys. Rev. Research **2**, 013236 (2020).

[25] D. Werdehausen, T. Takayama, M. Höppner, G. Albrecht, A. W. Rost, Y. Lu, D. Manske, H. Takagi, and S. Kaiser, Sci. Adv. **4**, eaap8652 (2018).

[26] B. Zenker, H. Fehske, and H. Beck, Phys. Rev. B **90**, 195118 (2014).

[27] T. Kaneko, K. Seki, and Y. Ohta, Phys. Rev. B **85**, 165135 (2012).

[28] K. Seki, Y. Wakisaka, T. Kaneko, T. Toriyama, T. Konishi, T. Sudayama, N. L. Saini, M. Arita, H. Namatame, M. Taniguchi, N. Katayama, M. Nohara, H. Takagi, T. Mizokawa, and Y. Ohta, Phys. Rev. B **90**, 155116 (2014).

[29] L. Butov, A. Gossard, and D. Chemla, Nature (London) **418**, 751 (2002).

[30] Z. Sun and A. J. Millis, Phys. Rev. B **102**, 041110(R) (2020).

[31] D. Nandi, A. Finck, J. Eisenstein, L. Pfeiffer, and K. West, Nature (London) **488**, 481 (2012).

[32] L. Ma, P. X. Nguyen, Z. Wang, Y. Zeng, K. Watanabe, T. Taniguchi, A. H. MacDonald, K. F. Mak, and J. Shan, Nature (London) **598**, 585 (2021).

[33] K. Seki, R. Eder, and Y. Ohta, Phys. Rev. B **84**, 245106 (2011).

[34] G. Mazza, M. Rösner, L. Windgätter, S. Latini, H. Hübener, A. J. Millis, A. Rubio, and A. Georges, Phys. Rev. Lett. **124**, 197601 (2020).

[35] T. I. Larkin, A. N. Yaresko, D. Pröpper, K. A. Kikoin, Y. F. Lu, T. Takayama, Y.-L. Mathis, A. W. Rost, H. Takagi, B. Keimer, and A. V. Boris, Phys. Rev. B **95**, 195144 (2017).

[36] T. I. Larkin, R. D. Dawson, M. Höppner, T. Takayama, M. Isobe, Y.-L. Mathis, H. Takagi, B. Keimer, and A. V. Boris, Phys. Rev. B **98**, 125113 (2018).

[37] H. M. Bretscher, P. Andrich, Y. Murakami, D. Golež, B. Remez, P. Telang, A. Singh, L. Harnagea, N. R. Cooper, A. J. Millis *et al.*, Sci. Adv. **7**, eabd6147 (2021).

[38] K. Okazaki, Y. Ogawa, T. Suzuki, T. Yamamoto, T. Someya, S. Michimae, M. Watanabe, Y. Lu, M. Nohara, H. Takagi *et al.*, Nat. Commun. **9**, 4322 (2018).

[39] T. Tang, H. Wang, S. Duan, Y. Yang, C. Huang, Y. Guo, D. Qian, and W. Zhang, Phys. Rev. B **101**, 235148 (2020).

[40] K. Sugimoto, S. Nishimoto, T. Kaneko, and Y. Ohta, Phys. Rev. Lett. **120**, 247602 (2018).

[41] A. Subedi, Phys. Rev. Materials **4**, 083601 (2020).

[42] L. Windgätter, M. Rösner, G. Mazza, H. Hübener, A. Georges, A. J. Millis, S. Latini, and A. Rubio, npj Comput. Materials **7**, 210 (2021).

[43] D. Golež, Z. Sun, Y. Murakami, A. Georges, and A. J. Millis, Phys. Rev. Lett. **125**, 257601 (2020).

[44] Y. Murakami, D. Golež, T. Kaneko, A. Koga, A. J. Millis, and P. Werner, Phys. Rev. B **101**, 195118 (2020).

[45] Y. Murakami, D. Golež, M. Eckstein, and P. Werner, Phys. Rev. Lett. **119**, 247601 (2017).

[46] Y. Tanaka, M. Daira, and K. Yonemitsu, Phys. Rev. B **97**, 115105 (2018).

[47] T. Tanabe, K. Sugimoto, and Y. Ohta, Phys. Rev. B **98**, 235127 (2018).

[48] R. Fujiuchi, T. Kaneko, Y. Ohta, and S. Yunoki, Phys. Rev. B **100**, 045121 (2019).

[49] F. Boschini, E. H. da Silva Neto, E. Razzoli, M. Zonno, S. Peli, R. P. Day, M. Michiardi, M. Schneider, B. Zwartsenberg, P. Nigge, R. D. Zhong, J. Schneeloch, G. D. Gu, S. Zhdanovich, A. K. Mills, G. Levy, D. J. Jones, C. Giannetti, and A. Damascelli, Nat. Mater. **17**, 416 (2018).

[50] T. Kaneko and Y. Ohta, J. Phys. Soc. Jpn. **83**, 024711 (2014).

[51] B. Zenker, D. Ihle, F. X. Bronold, and H. Fehske, Phys. Rev. B **85**, 121102(R) (2012).

[52] See Supplemental Material at http://link.aps.org/supplemental/10.1103/PhysRevB.106.L121106 for (i) a detailed description of the theoretical model, the evaluation of the photoemission spectrum and method, (ii) an analysis of photoemission changes at higher momenta, and (iii) an experimental data analysis and photodoping estimations, which includes Refs. [58–60].

[53] T. Suzuki, Y. Shinohara, Y. Lu, M. Watanabe, J. Xu, K. L. Ishikawa, H. Takagi, M. Nohara, N. Katayama, H. Sawa, M. Fujisawa, T. Kanai, J. Itatani, T. Mizokawa, S. Shin, and K. Okazaki, Phys. Rev. B **103**, L121105 (2021).

[54] A. Melnikov, O. Misochko, and S. Chekalin, Phys. Lett. A **375**, 2017 (2011).

[55] J. Li, D. Golez, G. Mazza, A. J. Millis, A. Georges, and M. Eckstein, Phys. Rev. B **101**, 205140 (2020).

[56] D. Golež, M. Eckstein, and P. Werner, Phys. Rev. B **100**, 235117 (2019).

[57] O. Dmytruk and M. Schiró, Phys. Rev. B **103**, 075131 (2021).

[58] T. Saha, D. Golež, G. De Ninno, J. Mravlje, Y. Murakami, B. Ressel, M. Stupar, and P. R. Ribič, Phys. Rev. B **103**, 144304 (2021).

[59] K. Matsubayashi, H. Okamura, T. Mizokawa, N. Katayama, A. Nakano, H. Sawa, T. Kaneko, T. Toriyama, T. Konishi, Y. Ohta *et al.*, J. Phys. Soc. Jpn. **90**, 074706 (2021).

[60] M. Schüler, D. Golež, Y. Murakami, N. Bittner, A. Herrmann, H. U. R. Strand, P. Werner, and M. Eckstein, Comput. Phys. Commun. **257**, 107484 (2020).